Engineering Applications of Jet Impingement Associated with Vertical Launching System Design

Seung-Kyu Hong* and Kwang-Seop Lee**
Agency for Defence Development
P.O. Box 35-3, Taejon, Korea 305-600

Abstract

In the course of missile system design, jet plume impingement is encountered in designing airframe as well as launchers, requiring careful investigation of its effect on the system. In the present paper, recent works on such topic are presented to demonstrate usefulness of CFD results in helping design the hardware. The jet impinging flow structure exhibits such complex nature as shock shell, plate shock and Mach disk depending on the flow parameters. The main parameters are the ratio of the jet pressure to the ambient pressure and the distance between the nozzle and the wall. In the current application, the nozzle contour and the pressure ratio are held fixed, but the jet impinging distance is varied to illuminate the characteristics of the jet plume with the distance. The same methodology is then applied to a complex vertical launcher system (VLS), capturing its flow structure and major design parameter. These applications involving jets are thus hoped to demonstrate the usefulness and value of CFD in designing a complex structure in the real engineering environment.

Key Word : jet impingement, CFDS scheme, VLS internal flow, VLS system design

Introduction

Supersonic jets occur in the exhausts from rocket motors and in various other situations. When the jets impinge on solid objects, such as parts of a missile launcher or the ground surface, high temperature and pressure loads can be produced. And these impingement flows are generally found to be extremely complex. The key feature of the flow field is a plate shock near the opposing wall. Between the plate shock and the solid surface is a region of subsonic and transonic flow similar to the shock layer produced by a blunt body in supersonic flow. The study of the jet and its structure has been conducted for many years both experimentally [1]-[12] and numerically [13]-[20]. Kitamura and Iwamoto [17] studied numerically supersonic impingement jet using axi-symmetric assumptions. And Sakakibra and Iwamoto [18] also investigated numerical study of oscillation mechanism for the under-expanded jet impinging on plate. They showed flow fields for different nozzle-plate spacing, uncovering pressure oscillation, frequency, and separation bubble. Recently, Hong and Lee [19] presented numerical simulations of jet plume impingement onto a duct using Navier-Stokes equations. Lee et al [20] also gave numerical solutions of a VLS type internal missile launcher including supersonic jet impingement.

VLS-type flow patterns are extremely complex and hard to obtain numerical solutions [21]. Specific review for each of these works will be omitted here for brevity except to mention that

* Principal Researcher
E-mail : skhong99@kornet.net, TEL: 042-821-4477, FAX: 042-821-2224
** Senior Researcher

fully three-dimensional Navier-Stokes simulations have rarely been carried out despite the wealth of research activities.

In the current presentation, dependency of jet impingement flow structure on the nozzle-plate distance was examined while the other parameters were fixed. Also attention is paid to see how well steady-state method fairs compared to unsteady version of the code. The steady-state version with variable CFL number is quite helpful in cutting down the computational turn-around time to provide timely data for the system engineers. A validation case was added to show the accuracy of present method against a well-known experiment [8]. VLS flow was then computed, yielding vital flow information for system designers and manufacturers.

Numerical Method

The CFDS, termed as the Characteristic Flux Difference Splitting, numerical method for the three-dimensional Navier-Stokes has been applied to various complex flows and validated over the past few years [22]. The CFDS method shares common flux-difference ideas with those in Ref. [23] and Ref. [24]. Here for the sake of introduction, a brief description is given; details can be referred to Ref. [22].

The governing Navier-Stokes equations employed in the generalized coordinate system (ξ, η, ϕ) are expressed for the conservative variable vector as

$$J^{-1}\frac{\partial Q}{\partial t}+\frac{\partial}{\partial \xi}(\widehat{F}+\widehat{F_v})+\frac{\partial}{\partial \eta}(\widehat{G}+\widehat{G_v})+\frac{\partial}{\partial \phi}(\widehat{H}+\widehat{H_v})=0 \tag{1}$$

where J^{-1} is the Jacobian of the transformation, Q is the conservative variable vector, $\widehat{F}$, $\widehat{G}$ and $\widehat{H}$ are inviscid flux vectors, and $\widehat{F_v}$, $\widehat{G_v}$ and $\widehat{H_v}$ are viscous flux vectors. The inviscid fluxes are linearized and split for upwind discretizations by

$$\triangle_{\xi}F=\widetilde{A}\triangle Q=(\widetilde{A}^{+}+\widetilde{A}^{-})\triangle Q \text{ and } \widetilde{\mathbf{A}}^{\pm}=\overline{\mathbf{M}}\,\overline{\mathbf{T}}\,\overline{\Lambda}^{\pm}\,\overline{\mathbf{M}}^{-1}\,\overline{\mathbf{T}}^{-1} \tag{2}$$

yielding

$$J^{-1}\frac{\delta Q}{\Delta t}+\widetilde{A}^{+}\nabla_{\xi}Q+\widetilde{A}^{-}\triangle_{\xi}Q+\widetilde{B}^{+}\nabla_{\eta}Q+\widetilde{B}^{-}\triangle_{\eta}Q+\widetilde{C}^{+}\nabla_{\phi}Q+\widetilde{C}^{-}\triangle_{\phi}Q=0 \tag{3}$$

where $\delta Q=Q^{(n+1)}-Q^{(n)}$ and the overbar means the associated variable is space-averaged over the interval, [j, j+1]. $\overline{M}$ or $\overline{M}^{-1}$ is a transformation matrix between the conservative variable vector Q and the primitive variable vector, say, $\widetilde{Q}$. $\overline{T}$ or $\overline{T}^{-1}$ is defined to be a transformation matrix between the primitive variable vector $\widetilde{Q}$ and the characteristic variable vector, say, $\widetilde{\widetilde{Q}}$.

The strength of current CFDS formulation is to enable one to switch the difference equation from the conservation form

$$\frac{J^{-1}}{\Delta t}\delta Q+\overline{M}\,\overline{T}\,\overline{\Lambda}\,\overline{M}^{-1}\,\overline{T}^{-1}\triangle Q=0 \tag{4}$$

to characteristic form

$$\frac{J^{-1}}{\Delta t}\delta\widetilde{\widetilde{Q}}+\overline{\Lambda}\triangle\widetilde{\widetilde{Q}}=0 \tag{5}$$

rather easily written here for one-dimensional case for the sake of simplicity. When the eigenvalue becomes zero in Eq. (5), there is no convective wave information traveling to that point as occurs in the stagnation line. Since the CFDS formulation also splits the eigenvalue as

$$\Lambda=\Lambda^{+}+\Lambda^{-1} \tag{6}$$

this splitting is also susceptible to carbuncle problem [25-28] when Λ becomes zero. Thus it is necessary to prevent the eigenvalue component from becoming zero. This has been done via

$$\lambda = \lambda^{+} + \lambda^{-1} = (\lambda^{+} + \varepsilon) + (\lambda^{-} + \varepsilon) \tag{7}$$

with a proper choice of ε in the literature. An alternative formulation for the flux term instead of Eq. (2) to cure the shock instability is proposed:

$$\triangle_{\xi} \boldsymbol{F} = \boldsymbol{Fl}_{\frac{1}{2}} - \boldsymbol{Fl}_{-\frac{1}{2}} \tag{8}$$

where

$$\boldsymbol{Fl}_{\frac{1}{2}} = \frac{1}{2}[\boldsymbol{F}_j + \boldsymbol{F}_{j+1} - |\widetilde{\boldsymbol{A}}|(\boldsymbol{Q}_{j+1} - \boldsymbol{Q}_j)] \tag{9}$$

Here, $\widetilde{\boldsymbol{A}}$ is the same form in Eq. (2). The last term Eq. (9) $|\widetilde{\boldsymbol{A}}|(\boldsymbol{Q}_{j+1} - \boldsymbol{Q}_j)$ means numerical dissipation and $|\widetilde{\boldsymbol{A}}|$ equals $\overline{\boldsymbol{M}}\,\overline{\boldsymbol{T}}\,\overline{|\Lambda|}\,\overline{\boldsymbol{M}}^{-1}\,\overline{\boldsymbol{T}}^{-1}$. The flux definition in Eq. (9) is very similar in form to the Roe's flux definition. In the present study for supersonic jet impingement calculations, the entropy fixing formula in Eq. (9) employed are

$$|\lambda| = \left(\frac{\lambda^2 + \varepsilon^2}{2\varepsilon}\right) \text{ if } |\lambda| < \varepsilon, \text{ and} \tag{10}$$

with ε=constant.

This entropy fixing is used when grid aligned normal shock is detected. However, the original formulation in Eq. (2) is used for other grid points. For turbulent flow effect, Baldwin-Lomax model is employed.

Results and Discussions on Jet Impingement

Supersonic jet impingement cases are run for a chamber condition of pressure Pt=1200 psia and temperature Tt=2950 K, respectively. The pressure ratio Pr is 1.87, the exit Mach is 2.93 and the height H is variable. Figure 1 shows the jet impingement layout with the nozzle diameter of D=32.6 mm, and the nozzle-plate spacing H. The three main parameters are Mach number at the nozzle exit plane, the pressure ratio between the jet exit plane and the ambient, and the distance between the nozzle and the wall. For the present problem, the computational grid

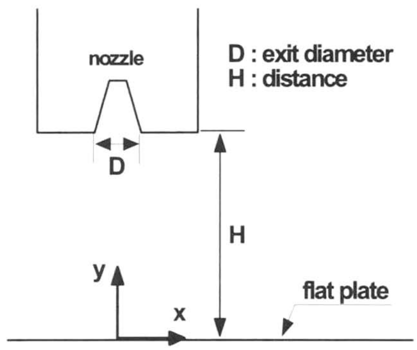

Fig. 1. Computational model.

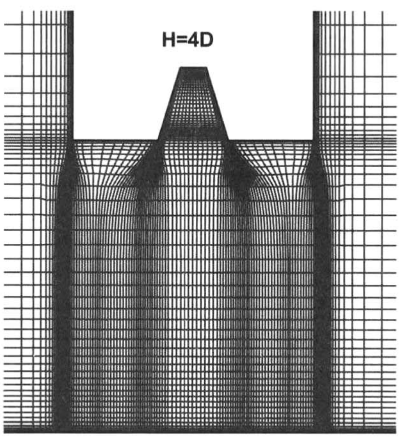

Fig. 2. (a) Grid topology in symmetric plane.

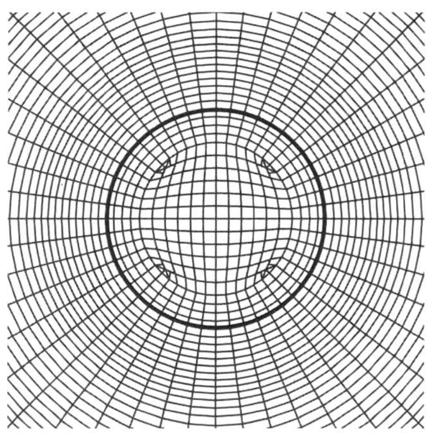

Fig. 2. (b) Grid in cross sectional plane.

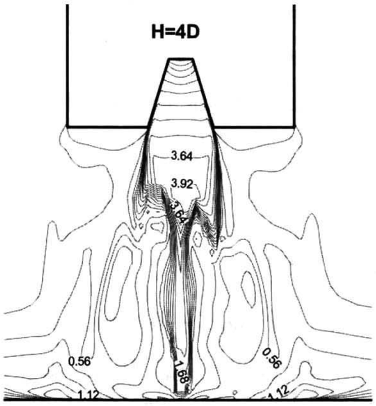

Fig. 3. Mach contours in symmetric plane without eigenvalue fixing.

consists of 310,000 grid points and seven blocks. Also overlap grid technique is used at block interfaces. Figure 2(a) shows grid in symmetric plane and Fig. 2(b), in cross-sectional plane parallel to the plate. A circle with bold line as shown in Fig. 2(b) represents the size of nozzle exit. This grid system without singular line helps improve solution quality and convergence. The computation domain starts from the nozzle throat with Mach 1.0 condition. The boundary conditions of this nozzle throat are calculated from isentropic relations and perfect gas law.

The jet impinging distance H is varied with discreet values of 3D, 4D, 5D, and 6D to illuminate the characteristics of the jet plume with the distance, while Pr is fixed at 1.87. Figure 3 shows Mach number contours contaminated with shock instability, so-called "carbuncle phenomenon" in symmetric plane. When a supersonic jet plume exhausts against the plate, strong normal shock is formed upon the plate. If the grid system used in numerical computation is aligned with this normal shock, the shock instability occurs which is cured by fixing small eigenvalues in numerical dissipation terms in the flux. Figure 4 shows Mach contours displaying shock shell, plate shock and Mach disk for various H. As the distance H increases the shock structures are also changed, but the distance between the plate and standing normal plate shock remains nearly the same.

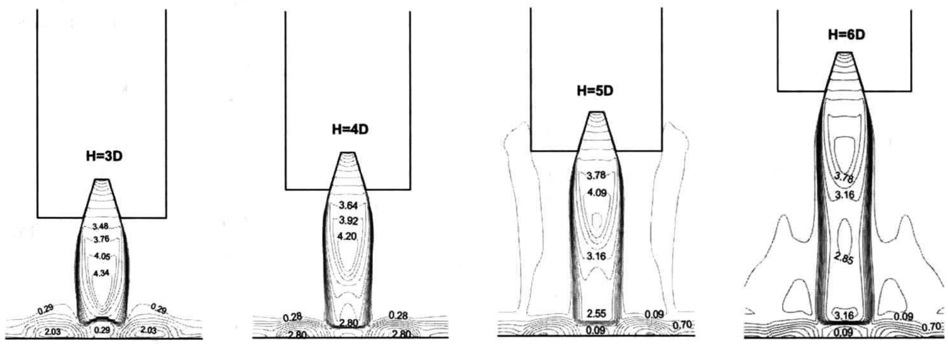

(a) H=3D (b) H=4D (c) H=5D (d) H=6D

Fig. 4. Mach contours in symmetric plane for various distance H.

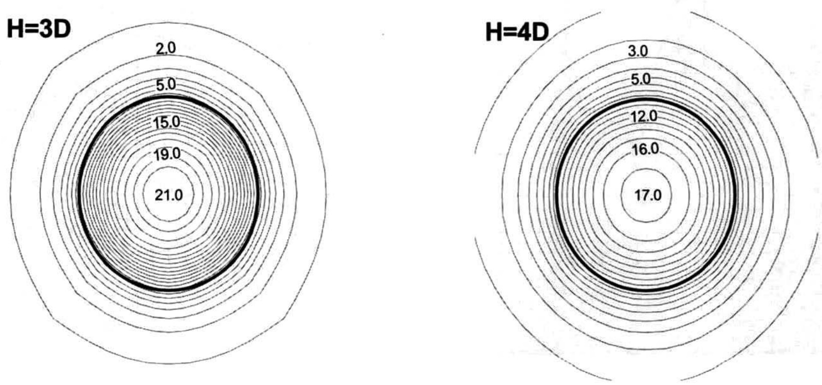

(a) H=3D (b) H=4D

Fig. 5. Pressure distributions on the flat plate (in atmospheric unit.)

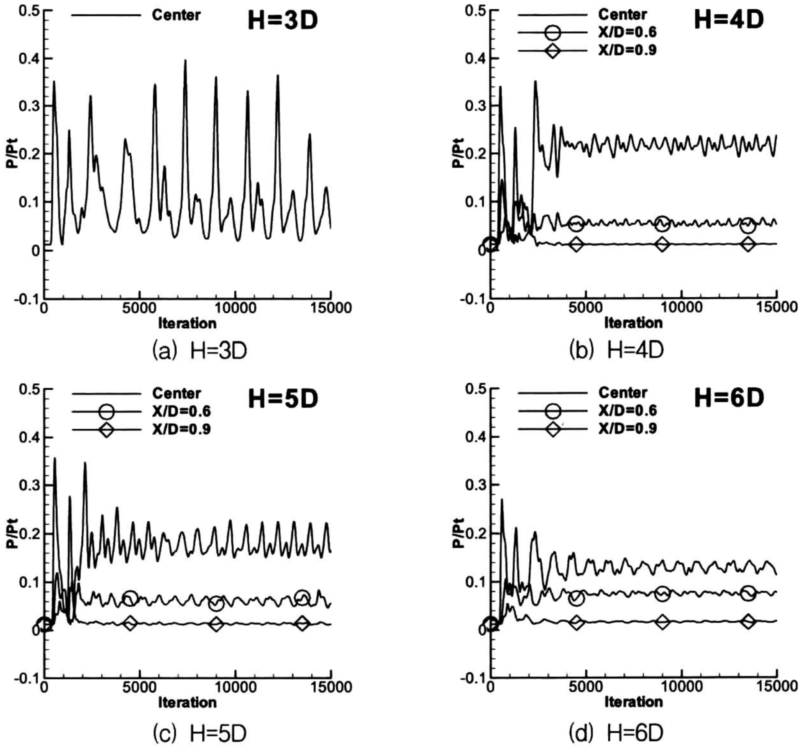

(a) H=3D (b) H=4D

(c) H=5D (d) H=6D

Fig. 6. Pressure history for different heights of H.

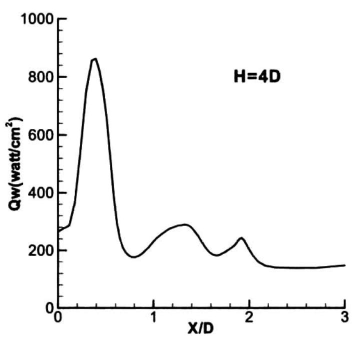

Fig. 7. Heat flux distributions in radial direction for H=4D.

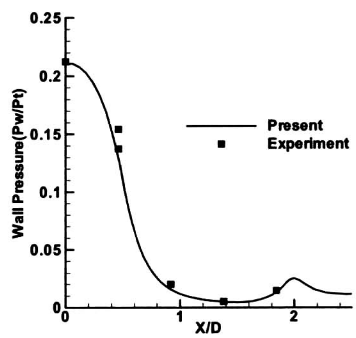

Fig. 8. Pressure distributions in radial direction for H=4D.

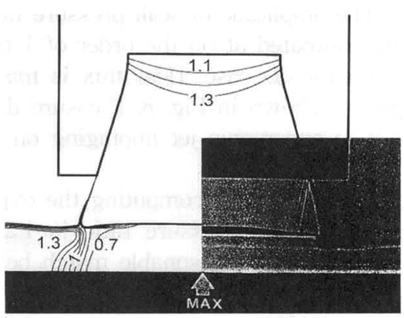

Fig. 9. Mach contours in symmetric plane for H=0.5D, Left: present computation, Right: experiment [8].

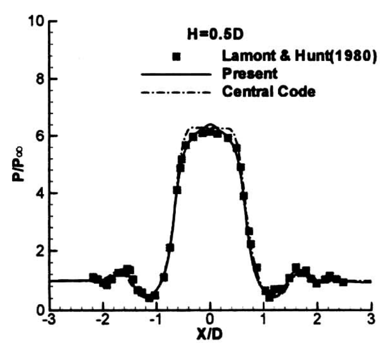

Fig. 10. Pressure distributions in radial direction for H=0.5D.

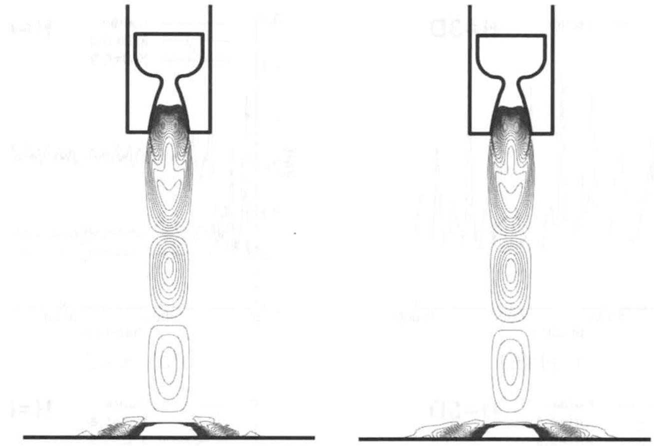

(a) unsteady solution (b) steady solution

Fig. 11. Comparison of pressure contours between unsteady and steady solution.

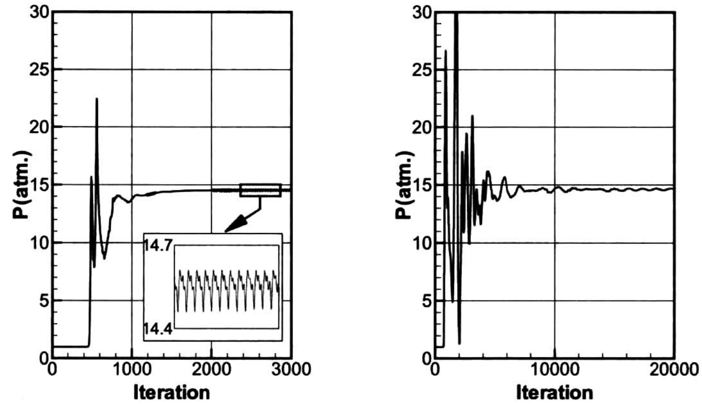

(a) unsteady solution (b) steady solution

Fig. 12. Pressure history comparison between unsteady and steady solution.

Pressure distributions on the flat plate are presented in Fig. 5 corresponding to H=3D and 4D. Pressure contours form exact circle in spite of using the rectangular grid in the core zone. Figure 6 represents pressure history as a function of numerical iterations. The unsteady nature of wall pressure fluctuations due to bouncing of the plate shock is uncovered for high pressure ratio of 1.87. As the plate is placed closer to the nozzle, the pressure fluctuates more vigorously and oscillates with large amplitude with respect to a mean value. The maximum pressure level at the plate is achieved when the distance is about 4D high. The amplitude of wall pressure fluctuations subsides as the distance increases; the frequency being estimated at on the order of 1 to 10 kHz. Figure 7 shows heat flux distributions in radial direction for 4D case. Heat flux is maximum at about X/D=0.5 and pressure drops rapidly in this region as shown in Fig. 8. Pressure distribution in the radial direction in Fig. 8 shows a typical pattern in supersonic jet impinging on flat plate, with the single peak at the jet center.

Accuracy of the forgoing results is also indirectly verified from computing the experimental flow of Lamont and Hunt [8], where the exit Mach is 2.2, the pressure ratio is 1.2, and the nozzle-plate distance is 0.5D. Comparisons in Figs. 9 and 10 show reasonable match between the computed and the experiment.

A second motor plume with the chamber pressure of 1500 psia, temperature of 2970K and nozzle diameter of 18.2 cm was computed. The pressure ratio is 2.33, the exit Mach is 2.93 and the height H is 7.34D. Purpose is to compare the steady-state solutions obtained with variable

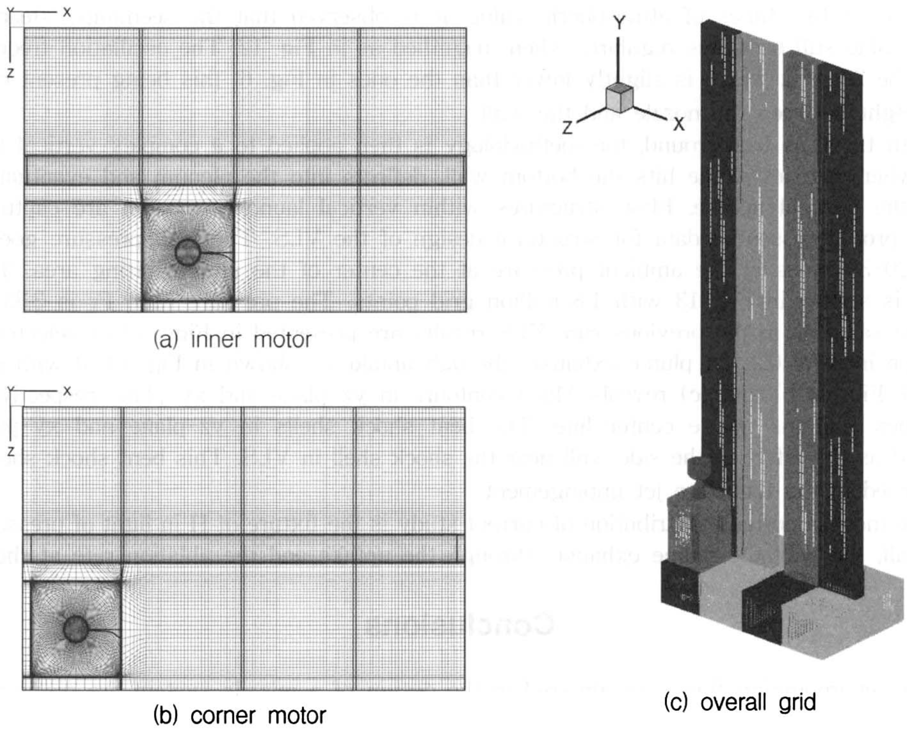

Fig. 13. Computational grid topology for VLS.

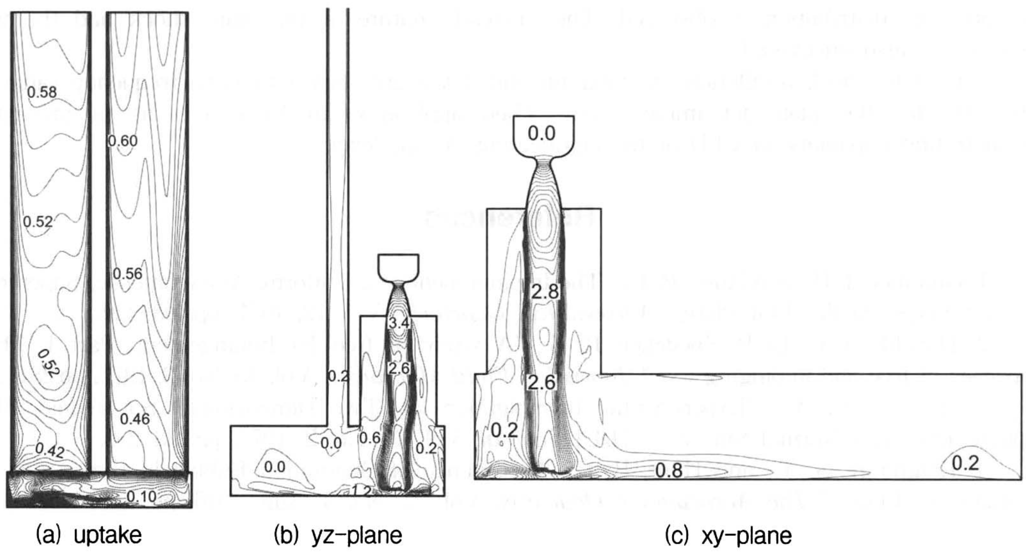

Fig. 14. Mach contours in VLS internal planes with Mach interval 0.2.

CFL number for different grid spacing with the time-accurate unsteady solutions using the inner iterations [29], displaying good agreement between the two sets of numerical solutions. The number of grid points are 800,000 due to increased height between the nozzle and the wall. Figure 11 compares the pressure contours which are plotted with 0.06 interval between 0 and 3 atm. The unsteady calculation utilizes 20 sub-iterations. Figure 12 also compares the convergence history of wall pressure at the center side by side. Initially the steady code solutions display more violent behavior than the unsteady code solutions, but overall the two sets of solutions converge to the same value of 14.5 times of atmospheric value. It is observed that the seemingly steady-state pressure value still oscillates regularly when magnified as in Fig. 12. The oscillation frequency is found to be 2.8 kHz which is slightly lower than the ones in Fig. 6; this being present case has longer height between the nozzle and the wall.

With these as background, the methodology is then applied to a complex vertical launcher system where the jet plume hits the bottom wall, deflects into the plenum and eventually exits through the vertical uptake. Flow structures within vertical launcher system are captured and solutions provide essential data for structural design of the VLS. The wall pressure goes up as high as 20-30 times of the ambient pressure at the center of the plume-hitting area. The grid topology is shown in Fig. 13 with 1.8 million grid points. The pressure ratio Pr is 2.33 and H, 7.34D; the same as in the previous run. VLS results are presented in Figs. 14 at selected planes with Mach interval 0.2. Jet plume exhausts through uptake as shown in Fig. 14(a) with speed of Mach 0.6. Fig. 14(b) and (c) reveals Mach contours in yz-plane and xy-plane respectively and both planes contains nozzle center line. The bent shock shells in yz-plane and xy-plane are considered as the effect of the side wall near the shock shell in VLS. This bent shock shells were not observed in the flat plate jet impingement.

The most important contribution of current study is the fixture of H in light of pressure level at the wall, the way the plume exhausts through the uptake and the ablation rate at the wall.

Conclusions

The jet impinging flows encountered in the design of a missile system are discussed with the purpose of uncovering physics associated with the flow and providing vital data for system engineers. The jet impingement creates the plate shock which may be difficult to capture with Roe-type flux-difference method. Depending on the nozzle-wall distance, single or double peak wall pressure distribution is observed. The unsteady nature of the plate shock and the wall pressure are also uncovered.

The plate shock oscillations moving up and down are shown to have frequency range of 1-10 kHz for flat plate jet impingement. Then application to VLS flow as is presented, demonstrating capability of CFD at the engineering design level.

References

1. Gummer, J. H., and Hunt, B. L., "The Impingement of a Uniform, Axisymmetric, Supersonic Jet on a Perpendicular Flat Plate," *Aeronautical Quarterly*, Vol. 12, 1971, pp.403-420.

2. Donaldson, C. DUP, Snedeker, R. S., "A study of free Jet Impingement. Part 1. Mean properties of free and impinging jets," *Journal of Fluid Mechanics*, Vol. 45, No. 2, 1971, pp.281-319.

3. Knight, C. V., "Experimental Investigation of Two-Dimensional, Supersonic Flow Impingement on a Normal Surface," *AIAA Journal*, Vol. 11, No. 2, 1973, pp.233-235.

4. Kalghatgi, G. T., and Hunt, B. L., "Occurrence of Stagnation Bubble in Supersonic Jet Impingement Flows," *The Aeronautical Quarterly*, Vol. 27, No. 3, Aug. 1976, pp. 169-185.

5. Lamont, P. J., and Hunt, B.L., "The Impingement of Underexpanded axisymmetric jets on Wedges," *Journal of Fluid Mechanics*, Vol. 76, part 2, 1976, pp. 307-336.

6. Zien, T.F., and Driftmyer, R. T., "Two-Dimensional Supersonic Jet Impingement on a Flat Plate," *AIAA Journal*, Vol. 17, No. 1, 1979, pp. 4-5.

7. Pamadi, B.L., "On the Impingement of Supersonic Jet on a Normal Flat Surface," *Aeronautical Quarterly*, 1982, pp.199-218.

8. Lamont, P. J., and Hunt, B.L., "The Impingement of Under-expanded Jet Interaction with a Plane Obstacle," *Journal of Fluid Mechanics*, Vol. 100, No. 3, 1980, pp.471-511.

9. Iwamoto, J., "Impingement of Under-Expanded Jets on a Flat Plate," *Journal of Fluid Engineering*, Vol. 112, No. 2, June 1990, pp. 179-184.

10. Masuda, W. and Moriyama, E., "Aerodynamic Characteristics of Underexpanded Coaxial Impinging Jets," *JSME International Journal*, Series B, Vol. 37, No. 4, 1994, pp.769-775.

11. Al-Qutub, A. M., and Budair, M. O., "Experiments of the Flow Over a Flat Surface Impinged by a Supersonic jet," AIAA Paper 95-2935.

12. Alvi, F.S., and Iyer, K.G., "Mean and Unsteady Flowfield Properties of Supersonic Impinging Jets with Lift Plates," AIAA Paper 99-1829, 5th AIAA/CEAS Aeroacoustics Conference, 10-12 May 1999.

13. Rubel, A., "Inviscid Axisymmeetric Jet Impingement with Recirculating Stagnation Regions," *AIAA Journal*, Vol. 21, No. 3, March 1983, pp.351-357.

14. Rizk, M.H. and Menon, S., "Numerical Simulation of Impinging Jets," AIAA 24th Aerospace Science Meeting, Jan.6-9, 1986/Reno, Nevada, AIAA Paper 86-0279.

15. Kim, K. H., and Chang, K. S., "Three-Dimensional Structure of a Supersonic Jet Impinging on an Inclined Plate," *Journal of Spacecraft and Rockets*, Vol. 31, No.5, Sep.-Oct., 1994, pp.778-782.

16. Chow, W.L., Ke, Z.P., and Lu, J.Q., "The Interaction between a Jet and a Flat Plate - an Inviscid Analysis," *Journal of Fluids Engineering*, Vol. 117, 1995, pp. 623-627.

17. Kitamura, S., and Iwamoto, J., "Numerical Analysis of Supersonic Impinging Jet," *Trans. Japan Soc. Aero. Space Sci.* Vol. 41, No. 132, 1998, pp.57-64.

18. Sakakibrara, Y., and Iwamoto, J., "Numerical Study of Oscillation Mechanism in Uderexpanded Jet Impinging on Plate," *Journal of Fluids Engineering*, Vol. 120, Sep. 1998, pp. 477-481.

19. S. K. Hong and K. S. Lee, "Simulation of Jet Plume Impinging onto a Duct," ISABE 97-7184, AIAA ISOABE (International Society for Air Breathing Engines) Symposium Papers, Sep. 7-12, 1997, Chattanooga, Tenneessee, USA, pp. 1359-1365.

20. K. S. Lee, S. K. Hong, S. O. Park, "Internal Flow Characteristics of VLS type Canister," Preceedings of The First National Congress on Fluids Engineering, Sep. 1-2, 2000, Muju, Korea.

21. J.J. Bertin, R.S. Bertin, and A. Yung, "The Launch-Tube Flow-Field for a Vertical Launching System," AIAA Paper 88-0332.

22. K. S. Lee, S. K. Hong and S. O. Park, "Improvement in Flux-Difference Splitting Algorithm for Accurate and Robust Flow Simulation," *Computational Fluid Dynamics Journal*, Japan, Vol. 10, No. 2, July 2001.

23. Lombard, C. K., Oliger, J., Yang, J. Y. and Davy, W. C., "Conservative Supra-Characteristics Method for Splitting the Hyperbolic Systems of Gasdynamics with Computed Boundaries for Real and Perfect Gases," AIAA-82-0837, June 1982.

24. Lombard, C. K., et al., "Multi-Dimensional Formulation of CSCM - An Upwind Flux Difference Eigenvector Split Method for the Compressible Navier-Stokes Equations", AIAA-83-1895, AIAA 6th CFD Conference, July 1983.

25. Quirk, J. J., "A Contribution to the Great Riemann Solver Debate," *Intl. J. for Numerical Methods in Fluids*, Vol. 18, 1994, pp. 555-574.

26. Richard Sanders, E. Morano, and M.C. Rduguert, "Multidimensional Dissipation for Upwind Schemes: Stability and Applications to Gas Dynamics," *Journal of Computational Physics*. 145, 1998, pp. 511-537.

27. Liou, M.S., "Mass Flux Schemes and Connection to Shock Instability," *Journal of Computational Physics*, 160, 2000, pp.623-648.

28. Pandolfi, M, and D'ambrosio, D., "Numerical Instabilities in Upwind Methods: Analysis and Cures for the 'Carbuncle' Phenomenon," *Journal of Computational Physics*, 166, 2001, pp. 271-301,.

29. K. Matsuno, "A Time-Accurate Iterative Scheme for Solving the Unsteady Compressible Flow Equations," AIAA-89-1992-CCCP, 1992.

30. Hong, S. K., Bardina, J., Lombard, C. K., Wang, D. and Codding, W., "A Matrix of 3-D Turbulent CFD Solutions for JI Control with Interacting Lateral and Attitude Thrusters," AIAA 91-2099, Sacramento, June 1991.